Supporting Information for "A novel wave breaking framework to estimate air-sea gas transfer velocities"

Sophia E. Brumer[1,a], Christopher J. Zappa[1]

[1]Lamont-Doherty Earth Observatory of Columbia University, Palisades, NY, USA.

[a]Now at Laboratoire d'Océanographie Physique et Spatiale, UMR 6523 CNRS-IFREMER-IRD-UBO, IUEM, Plouzané, France

Contents of this file

1. Text S1 to S4
2. Figures S1 to S2

Introduction

Text S1 provides more details regarding the breaking crest detection and tracking algorithm which should be sufficient to replicate it. It lists the functions of the Matlab image processing toolbox used. Note that the algorithm should be adapted to the spatial resolution of the imagery it is applied on.

Text S2 provides the equation for breaking crest length distribution scalings proposed in the literature (Deike and Melville, 2018; Sutherland and Melville, 2013). Both are based on the same dataset. Deike and Melville (2018) proposed a simplified form which is plotted in Figure S1 for HiWinGS conditions along with the breaking crest length distribution

determined in this study. A poor correspondence between the HiWinGS data and the scaling can be observed which may stem from the fundamentally different way breaking crest length distribution were computed in this study and those from which the scalings were derived. Addressing the difference is an active area of research which goes beyond the scope of this publication.

Text S3 recalls the main equations of the NOAA-COAREG algorithm. These can be found in Blomquist et al. (2017); Fairall et al. (2011) and references therein.

Text S4 discusses an alternate formulation of the bubble mediate transfer which accounts for suffocation which may occur in dense bubble plumes. It depends on an additional bubble plume characteristic which may be estimated from breaking crest length distribution and sea state statistics: the void fraction. Related geometric consideration of breaking waves and associated bubble plumes are illustrated in Figure S2. Due to an increased number of unknowns and scatter in results this formulation was not retained for the main framework.

Text S1. Steps of the breaking crest detection and tracking algorithm

1. Intrinsic and extrinsic image correction is applied to the images of a given video (frequency down-sampling is applied in this loop) which are re-gridded onto a regular x,y grid resulting in an image matrix $I(t, x, y)$ where t is the time dimension time
2. This matrix is differences with respect of time: *diffI = I(2:end,:,:)-I(1:end-1,:,:)*
3. diffI is converted into a binary matrix (1 for advancing crest, 0 for rest) based on an intensity threshold: *BW = im2bw(diffI./max(diffI(:)),0.6)*
4. Holes are filled using *BW = imfill(BW,'holes')*
5. The features in the image are dilated using *BW = imdilate(BW, strel('diamond',10))*
6. Pixels separated by only 1 pixel are connected using : *BW = bwmorph(BW,'bridge')*
7. Pixels are set to 1 if at least 5 pixels within a 3x3 neighbouring area are 1, if not they are set to 0 using: *BW = bwmorph(BW,'bridge')*
8. Holes are filled *BW = imfill(BW,'holes')*
9. The features in the image are eroded using *imerode(BW, strel('diamond',5))*
10. Individual features are identified and labeled: *[L,NO] = bwlabeln(BW,8);*
11. Region properties (area, orientation) are computed *L_props = regionprops(L,'area','orientation')*
12. Only features greater than the chosen area threshold (AreaThresh) are kept and labels are re-assigned: *BW = ismember(L,find([L_props.Area] > AreaThresh)); [L,NO] = bwlabeln(BW,8)*
13. Breaking crests are tracked from one differenced image pair to the next by matching features that evolve corresponding to to the criterion mentioned in section 3.1.

Text S2. Lambda scaling

Two scalings have been proposed for $\Lambda(c)$ for $c > c_{min}$ assuming a c^{-6} tail:

1. Deike and Melville (2018):

$$\Lambda(c) = 0.25 \frac{g}{\sqrt{gH_s}^3} \left(\frac{c}{\sqrt{gH_s}} \right)^{-6} \left(\frac{u_*}{\sqrt{gH_s}} \right)^{5/3} \tag{S1}$$

$$c_{min} = 0.85\sqrt{gH_s} \tag{S2}$$

2. Sutherland and Melville (2013):

$$\Lambda(c) = \frac{g}{c_p^3} \sqrt{\frac{u_*}{c_p}} \frac{c}{gH_s} \left(\frac{gHs}{c_p^2} \right)^{0.1} \tag{S3}$$

Figure S1 show how the scaling of Deike and Melville (2018) for the HiWinGS sea state conditions compares to the imagery derived breaking crest length distribution.

Text S3. The NOAA-COAREG algorithm

The key equations of the NOAA-COAREG algorithm are recalled in the following section. These were published in Blomquist et al. (2017); Fairall et al. (2011) and references therein. The gas transfer velocity is composed of an air- $(1/k_a)$ and a water-side resistance $(1/k_w)$:

$$k = (\alpha/k_a + 1/k_w)^{-1} \tag{S4}$$

The air-side transfer depends on the air friction velocity (u_*), the atmospheric velocity drag coefficient (C_d), and the Schmidt number for the gas in the air (Sc_a).

$$k_a = u_* / \left(13.3 Sc_a^{1/2} + C_d^{1/2} - 5 + \ln(Sc_a)/(2\kappa)\right) \tag{S5}$$

The water-side transfer is composed of a turbulent molecular transfer (k_{wt}) and a bubble mediated (k_b) one:

$$k_w = k_{wt} + k_b \tag{S6}$$

The turbulent molecular transfer formulation takes the cool skin buoyancy driven transfer at low wind though an empirical function Φ in addition to effects of the tangential wind stress:

$$k_{wt} = u_* / (\rho_w/\rho_a)^{1/2} / \left(13.3/(\mathcal{A}_{COAREG}\Phi) Sc^{1/2} + ln(z_w/\delta_w)/\kappa\right) \tag{S7}$$

Here z_w is set to 0.5 and the Schmidt number of the gas in water (Sc) to 660. The cool-skin thickness, δ_w, is computed in the iterative loop of the COARE algorithm as is Φ. The bubble mediated transfer formulation is that of Woolf (1997):

$$k_b = \mathcal{B}_{COAREG} \times 2450 W \alpha^{-1} \left(1 + \left(14 \alpha Sc^{-0.5}\right)^{1/1.2}\right)^{-1.2} \tag{S8}$$

The whitecap fraction W is parameterized as a function of wave-wind Reynolds number following Brumer et al. (2017):

$$W = 4.48 \times 10^{-6} \left(\frac{u_* H_s}{\nu_w} \right)^{0.90} /100 \tag{S9}$$

The two adjustment factors $\mathcal{A}_{COAREG}$ and $\mathcal{B}_{COAREG}$ are set to 1.2 and 3.8, respectively, based on the HiWinGS measurements (Blomquist et al., 2017).

Text S4. Accounting for suffocation

The model based on Eq. 5 does not account for the potential "suffocation" effect of bubbles within dense clouds. This effect was suggested to arise from the fact that bubbles evolve within a finite volume of water with relatively small interstitial space which has limited capacity to take up gases, thus restricting the bubble-mediated transfer (Woolf et al., 2007). An alternate form for k_b, labeled as the "dense plume model" was therefor proposed:

$$k_{b_{void}} \propto W \times X \frac{F_{a_{1\%}}}{\alpha}(1 + (X\chi)^{1/1.2})^{-1.2} \tag{S10}$$

with

$$X = \alpha F_{w_{1\%}}/(\alpha F_{w_{1\%}} + F_{a_{1\%}}) \tag{S11}$$

$F_{a_{1\%}}$ is the volume flux of air for 1% whitecap cover, i.e $F_{a_{1\%}} = F_a/W$, which Woolf et al. (2007) set to equal 24.5 cm hr^{-1}. $F_{w_{1\%}}$ is the volume flux of water within bubble plume relative to $F_{a_{1\%}}$ and is related to $F_{a_{1\%}}$ through the void fraction:

$$v = \frac{F_{a_{1\%}}}{F_{a_{1\%}} + F_{w_{1\%}}}. \tag{S12}$$

Thus:

$$F_{w_{1\%}} = \frac{F_{a_{1\%}}}{v} - F_{a_{1\%}} \tag{S13}$$

and

$$X = \frac{\alpha/v + \alpha}{\alpha/v + \alpha + 1} \tag{S14}$$

The void fraction for a given breaking wave (v_{br}) can be estimated from V_a, the surface area of active breaking (A_{br}), which is proportional to the breaking crest length times

the "swept out" length of the breaker ($L_{br} \times c_{br}t_{br}$, see Figure S2), and the depth of the bubble plume (h):

$$v_{br} = \frac{V_a}{A_{br}h} = b_{eff}\frac{B}{U_b g^2}\frac{L_{br}c_{br}^5}{L_{br}c_{br}t_{br}h} = b_{eff}\frac{B}{U_b g^2}\frac{c_{br}^4}{t_{br}h} \tag{S15}$$

The time averaged void fraction is then:

$$\overline{v} = \frac{\sum v_{br}t_{br}}{T} \tag{S16}$$

The bubble plume depth remains elusive, but may be assumed to be proportional to the significant wave height of the wind-sea ($H_{s_{ws}}$) or to the "swept out" length of the breaker ($c_{br}t_{br}$). Figure S2 illustrates the assumed geometry of a plunging breaker and the subsequent bubble plume. Recent work (Cifuentes-Lorenzen et al., 2020) suggests that the peak wave number k_p is a better predictor for the bubble plume depths based on acoustic backscatter measurements due to breaking waves in the Southern Ocean.

The three estimates are then given by:

1. assuming $h \propto H_{s_{ws}}$ (e.g., Rapp and Melville, 1990; Lamarre and Melville, 1991; Baldy and Bourguel, 1987):

$$\overline{v} \propto \frac{b_{eff}B}{H_{s_{ws}}TU_b g^2}\sum c_{br}^4. \tag{S17}$$

2. assuming $h \propto c_{br}t_{br}$ (e.g., Deike et al., 2016):

$$\overline{v} \propto \frac{b_{eff}B}{TU_b g^2}\sum \frac{c_{br}^3}{t_{br}}. \tag{S18}$$

3. assuming $h \propto f(k_p)$:

$$\overline{v} \propto \frac{b_{eff}B}{f(k_p)TU_b g^2}\sum c_{br}^4. \tag{S19}$$

Note that all three forms are independent of the breaking crest length and cannot be expressed in terms of moments of the breaking crest length distribution. They are however

straight forward to determine from the imagery during the processing to obtain $\Lambda(c)$. In light of recent modeling advances (Romero, 2019), breaking crest length distribution dependant formulations are of higher interest to the community. What is more, Eq. S10 contains more uncertainties than Eq. 5). Using the right hand side of Eq. S10, with the void fraction estimated based any of the above equations instead of K_b leads to very poor overall correlations ($r^2 \sim 0.1$) on account of the large scatter in $\overline{v}$.

References

Baldy, S. and Bourguel, M. (1987). Bubbles between the wave trough and wave crest levels. *Journal of Geophysical Research: Oceans*, 92(C3):2919–2929.

Blomquist, B. W., Brumer, S. E., Fairall, C. W., Huebert, B. J., Zappa, C. J., Brooks, I. M., Yang, M., Bariteau, L., Prytherch, J., Hare, J. E., Czerski, H., Matei, A., and Pascal, R. W. (2017). Wind speed and sea state dependencies of air-sea gas transfer: Results from the high wind speed gas exchange study (HiWinGS). *Journal of Geophysical Research: Oceans*, 122(10):8034–8062.

Brumer, S. E., Zappa, C. J., Brooks, I. M., Tamura, H., Brown, S. M., Blomquist, B., Fairall, C. W., and Cifuentes-Lorenzen, A. (2017). Whitecap coverage dependence on wind and wave statistics as observed during so gasex and hiwings. *Journal of Physical Oceanography*.

Cifuentes-Lorenzen, A., Zappa, C. J., Randolph, K. L., and Edson, J. B. (2020). Scaling the bubble penetration depth in the open ocean during the southern ocean gas exchange experiment 2008. In *Ocean Sciences Meeting*.

Deike, L. and Melville, W. K. (2018). Gas transfer by breaking waves. *Geophysical Research Letters*, 45(19):10,482–10,492.

Deike, L., Melville, W. K., and Popinet, S. (2016). Air entrainment and bubble statistics in breaking waves. *Journal of Fluid Mechanics*, 801:91–129.

Fairall, C. W., Yang, M., Bariteau, L., Edson, J. B., Helmig, D., McGillis, W., Pezoa, S., Hare, J. E., Huebert, B., and Blomquist, B. (2011). Implementation of the coupled ocean-atmosphere response experiment flux algorithm with CO_2, dimethyl sulfide, and

O_3. *Journal of Geophysical Research*, 116(C00F09):C00F09.

Lamarre, E. and Melville, W. K. (1991). Air entrainment and dissipation in breaking waves. *Nature*, 351(6326):469–72.

Rapp, R. J. and Melville, W. K. (1990). Laboratory measurements of deep-water breaking waves. *Philosophical Transactions of the Royal Society of London A*, 331(1622):735–800.

Romero, L. (2019). Distribution of surface wave breaking fronts. *Geophysical Research Letters*, 46(17-18):10463–10474.

Sutherland, P. and Melville, W. K. (2013). Field measurements and scaling of ocean surface wave-breaking statistics. *Geophysical Research Letters*, 40:3074–3079.

Woolf, D. K. (1997). *Bubbles and their role in air-sea gas exchange*, pages 173–206. Cambridge Univ Press, Cambridge, UK.

Woolf, D. K., Leifer, I. S., Nightingale, P. D., Rhee, T. S., Bowyer, P., Caulliez, G., de Leeuw, G., Larsen, S. E., Liddicoat, M., Baker, J., and Andreae, M. O. (2007). Modelling of bubble-mediated gas transfer: Fundamental principles and a laboratory test. *Journal of Marine Systems*, 66(1-4):71–91.

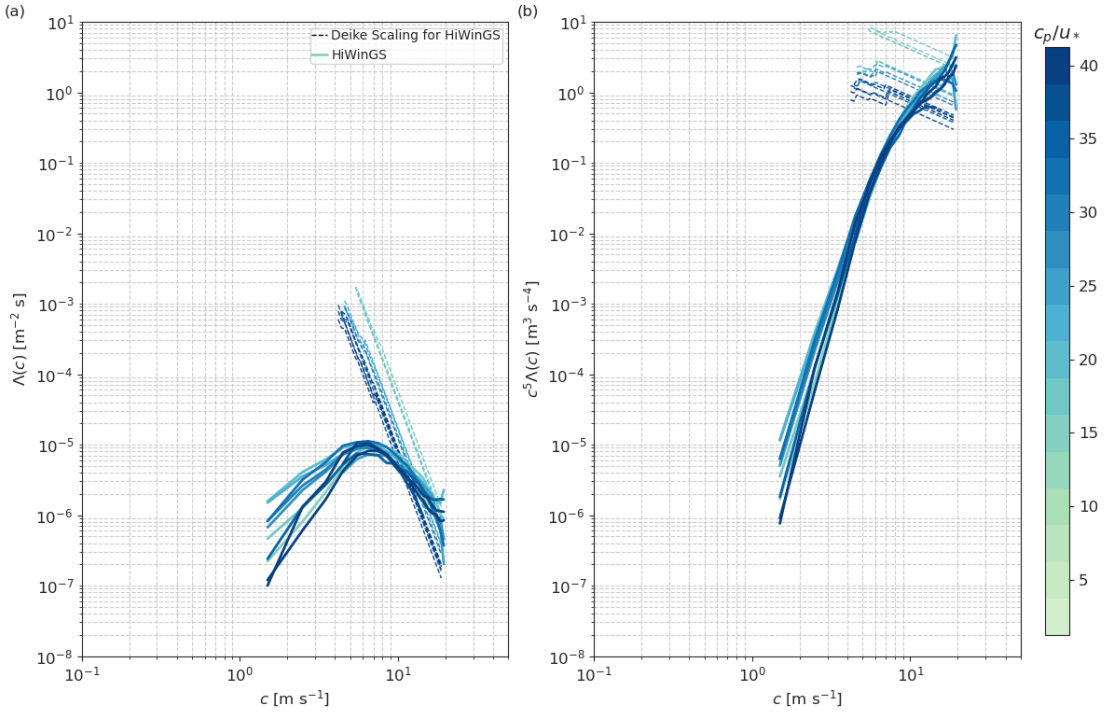

Figure S1. (a) Breaking crest length distributions and (b) their fifth moment as a function of the breaking crest speed color-coded by wave age ($\frac{c_p}{u_*}$). The HiWinGS data is plotted in solid lines while the corresponding Deike and Melville (2018) scaling is in dashed lines.

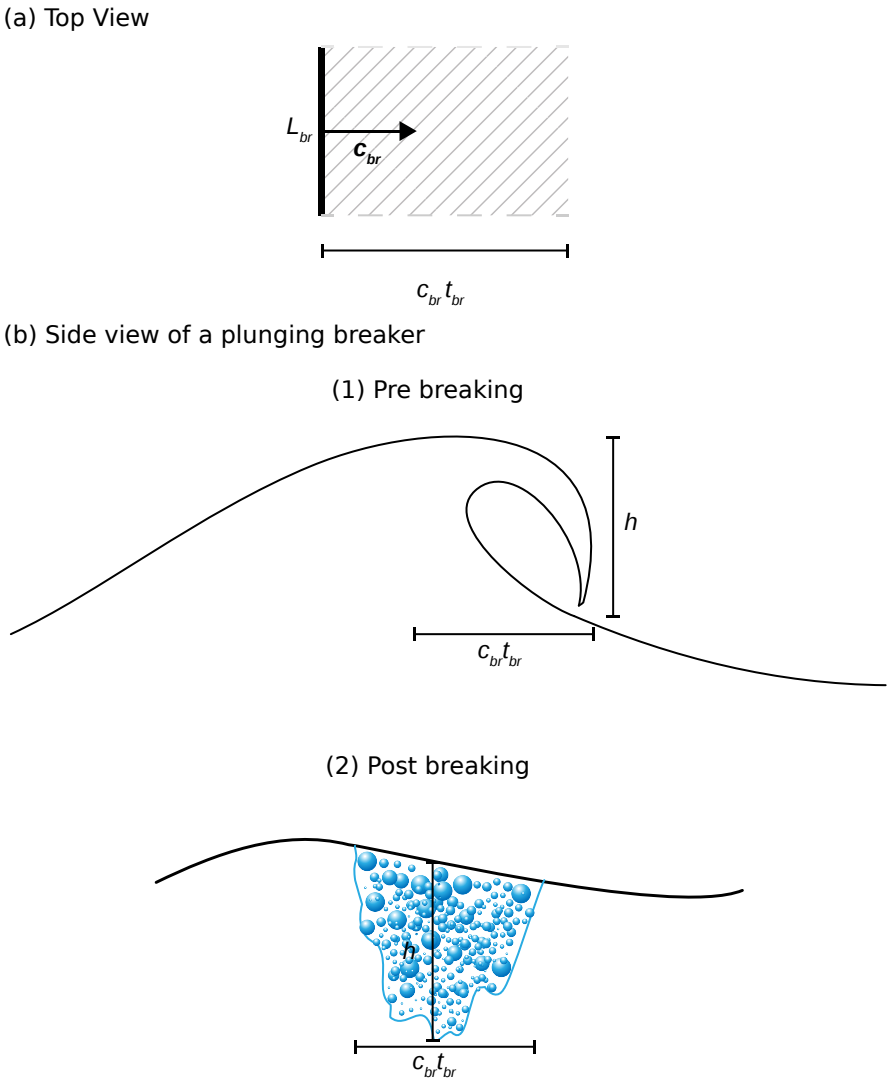

Figure S2. Sketch illustrating (a) the assumption that the swept out area is related to the length of breaking L_{br}, the translation $c_{br}t_{br}$ and (b) the assumed geometry of (1) a plunging breaker, and (2) the subsequent bubble plume.